Charged Surface Area of Maurocalcine Determines Its Interaction with the Skeletal Ryanodine Receptor

Balázs Lukács,* Mónika Sztretye,* János Almássy,* Sándor Sárközi,* Beatrix Dienes,* Kamel Mabrouk,§ Cecilia Simut,* László Szabó,*¶ Péter Szentesi,* Michel De Waard,†‡ Michel Ronjat,†‡ István Jóna,* and László Csernoch*

*Department of Physiology, Research Centre for Molecular Medicine, Medical and Health Science Centre, University of Debrecen, Debrecen, Hungary; †Institut National de la Santé et de la Recherche Médicale, U836, Grenoble, France; ‡Institut des Neurosciences, Université Joseph Fourier, Grenoble, France; §Universités D'Aix-Marseille 1, 2 et 3 Centre National de la Recherche Scientifique-Unite Mixte de Recherche 6517 "Chimie, Biologie et Radicaux Libres," Marseille, France; and ¶Department of Electrical Engineering, Sapientia Hungarian University of Transylvania, Targu Mures, Romania

ABSTRACT The 33 amino acid scorpion toxin maurocalcine (MCa) has been shown to modify the gating of the skeletal-type ryanodine receptor (RyR1). Here we explored the effects of MCa and its mutants ([Ala^{8}]MCa, [Ala^{19}]MCa, [Ala^{20}]MCa, [Ala^{22}]MCa, [Ala^{23}]MCa, and [Ala^{24}]MCa) on RyR1 incorporated into artificial lipid bilayers and on elementary calcium release events (ECRE) in rat and frog skeletal muscle fibers. The peptides induced long-lasting subconductance states (LLSS) on RyR1 that lasted for several seconds. However, their average length and frequency were decreased if the mutation was placed farther away in the 3D structure from the critical ^{24}Arg residue. The effect was strongly dependent on the direction of the current through the channel. If the direction was similar to that followed by calcium during release, the peptides were 8- to 10-fold less effective. In fibers long-lasting calcium release events were observed after the addition of the peptides. The average length of these events correlated well with the duration of LLSS. These data suggest that the effect of the peptide is governed by the large charged surface formed by residues Lys^{20}, Lys^{22}, Arg^{23}, Arg^{24}, and Lys^{8}. Our observations also indicate that the results from bilayer experiments mimic the in situ effects of MCa on RyR1.

INTRODUCTION

Excitation-contraction (EC) coupling in skeletal muscle fibers requires the functional interaction of two calcium channels, the dihydropyridine receptor (DHPR) and the ryanodine receptor (RyR1), residing in the transverse tubular membrane and the membrane of the terminal cisternae of the sarcoplasmic reticulum (SR), respectively. In amphibian skeletal muscle cells, Ca^{2+} release from SR has been proposed to result from the summation of calcium release events, termed sparks, corresponding to the opening of a discrete number of ryanodine receptors (1–3). In contrast, intact adult mammalian skeletal muscle fibers do not give rise to spontaneous Ca^{2+} release events (4). However, as was recently shown, a mild treatment of adult mammalian skeletal fibers with saponin provokes the appearance of Ca^{2+} release events with various morphology (5–7), long events with constant amplitude (called embers) (3), and sparks similar to those observed in frog skeletal muscle cells. It remains to be demonstrated, however, that these events are indeed the elementary building blocks of Ca^{2+} release in mammalian muscle, and that embers represent the opening of a single or a few but coupled (8) RyR1.

Three structurally related scorpion toxins—imperatoxin A (IpTxA), maurocalcine (MCa), and hemicalcin—have been shown to modify RyR1 Ca^{2+} channel properties in vitro (9–11). Two of them have already proved to be useful tools for studying EC coupling and elementary events of Ca^{2+} release. It was also demonstrated that MCa 1), induces Ca^{2+} release from SR vesicles; 2), strongly potentiates [^{3}H]ryanodine binding to SR vesicles; and 3), increases the open probability of the purified RyR1 (12,13). In cultured rat myotubes, MCa induces Ca^{2+} release via the ryanodine receptor but has no effect on the depolarization-evoked Ca^{2+} transient per se. In contrast, MCa does not induce any Ca^{2+} release or Ca^{2+} release events in intact adult mammalian fibers. On the other hand, in saponin-treated adult mammalian cells, MCa had a biphasic effect, inducing first a strong increase in calcium release event frequency and then the appearance of long-lasting embers (14). In addition, under voltage clamp conditions the peptide interfered with the repolarization-induced closure of RyRs, raising the possibility that the binding site of the peptide becomes accessible after the activation by DHPR (15).

Recent results have also drawn attention to the charged amino acid residues around position 24 in MCa as the possible interaction site for the peptide binding to RyR1 (13,14). It is not clear, however, whether alterations in the cluster of positive charges around residue 24 would simply lower the affinity of peptide binding to RyR1 or also have a functional effect on the interaction. It also remains to be experimentally confirmed

Submitted September 7, 2007, and accepted for publication June 3, 2008.

Balázs Lukács and Mónika Sztretye contributed equally to this work.

Address reprint requests to Dr. László Csernoch, Dept. of Physiology, University of Debrecen, PO Box 22, Debrecen, Hungary H-4012. Tel.: 36-52-416-634; Fax: 36-52-432-289; E-mail: csl@phys.dote.hu.

Cecilia Simut's present address is Department of Physics, University of Oradea, Oradea, Romania.

Editor: David S. Weiss.

0006-3495/08/10/3497/13 $2.00

doi: 10.1529/biophysj.107.120840

whether alterations seen on isolated channels incorporated into lipid bilayers will also appear under in situ conditions.

In this study we investigated the effects of different mutations of MCa on the Ca^{2+} release channel of SR and on the spontaneous Ca^{2+} release events in permeabilized adult skeletal muscle fibers from both amphibians and mammals. We show that MCa and its mutants induce, in a concentration-dependent manner, subconductance states in skeletal RyR when applied on the cytosolic side. Analysis of the concentration dependence of different mutants of the peptide suggests that the induction of these long-lasting subconductance states (LLSS) corresponds to a reversible binding and unbinding of MCa at a site that is accessible from the cytosolic side. These results strongly support the hypothesis that the effects of MCa depend on the charged surface region of the peptide.

Part of this work has been presented to the European Muscle Society (16).

MATERIALS AND METHODS

Chemical synthesis and peptide structure

MCa and its analogs were obtained by the solid-phase peptide synthesis (17) using an automated peptide synthesizer (model 433A, Applied Biosystems Inc., Foster City, CA, USA) as described previously (13). Analogues were obtained by point mutation, with Ala replacing one amino acid in the sequence of native-like MCa, and named [Ala^8]MCa, [Ala^{19}]MCa, [Ala^{20}]MCa, [Ala^{22}]MCa, [Ala^{23}]MCa, and [Ala^{24}]MCa. Three-dimensional (3D) structures of the peptide and its mutated analogs were calculated using the coordinates obtained from the Swiss Protein Data Bank, based on the NMR measurement in aqueous phase, using Swiss-Pdbviewer 3.7 (SP5) shareware software downloadable from the GalaxoSmithKline server (http://www.expasy.ch).

Preparation of heavy SR vesicles

Heavy SR (HSR) vesicles—containing vesicles formed from membrane fragments of the terminal cisternae of the SR—were isolated from rat skeletal muscle according to Lai and Meissner (18) with slight modifications (19). After a homogenization step in 100 mM NaCl, 20 mM EGTA, 20 mM Na-HEPES, pH = 7.5, first crude microsomes were collected by centrifugation at 40,000 × *g*. After the actomyosin contamination was removed by solubilization in 600 mM KCl, the microsome fraction was collected at 109,000 × *g*. The pellet was resuspended and loaded onto a 20–45% linear sucrose gradient. HSR vesicles were extracted from the 36–38% region of the continuous sucrose gradient, collected by centrifugation, and resuspended in 0.4 M sucrose, 10 mM K-PIPES, pH = 7.0. Protein concentration was measured by the Biuret method.

RyR1 Ca^{2+} channel reconstitution and single-channel recording analysis

Measurements of channel activity were carried out using purified RyR1 incorporated into planar lipid bilayers. RyR1 was purified from rat SR vesicles as previously described (20). The bilayers were formed using phosphatidylethanolamine, phosphatidylserine, and L-phosphatidylcholine in a ratio of 5:4:1 dissolved in *n*-decane up to the final lipid concentration of 20 mg/mL (21). Bilayers were formed across a 200 or 250 μm diameter aperture of a Delrin cap using a symmetrical buffer solution (in mM: 250 KCl, 0.1 EGTA, 0.15 $CaCl_2$, 20 PIPES, pH 7.2). A small aliquot of purified RyR1 was added into the chamber, which was defined as the *cis* (cytoplasmic) side, whereas the other chamber, labeled as the *trans* (luminal) side, was kept on ground potential. To ensure the orientation of the incorporated RyR1, we tested the effect of Ca^{2+} on both sides. After successful incorporation of the RyR1 channel, free calcium concentration in the *cis* chamber was adjusted to 238 nM by the addition of EGTA. Electrical signals were filtered at 1 kHz through an eight-pole low-pass Bessel filter and digitized at 3 kHz using Axopatch 200 and pCLAMP 6.03 (Axon Instruments, Union City, CA, USA). The total recording time in each experiment was 10–20 min for each experimental condition tested. After the conditions were changed, at least 5 min were allowed for equilibration, which appeared to be enough to reach the new equilibrium of the parameters. Single-channel measurements were carried out at 22 ± 1°C. The free Ca^{2+} concentration was calculated using the computer program and affinity constants published by Fabiato (22). Open probabilities were calculated using the common 50% criteria with a medial dead zone of 5%. Current amplitude distribution was analyzed using Origin software (Microcal Software, Northampton, MA, USA). The LLSS ratio was calculated as the fraction of time the channel spent in the LLSS from a given (usually several minutes long) total recording time.

Determination of the ATPase activity

ATPase activity was determined at 37°C by a coupled enzyme assay in a medium containing 100 mM KCl, 20 mM Tris-HCl, 5 mM $MgCl_2$, 5 mM ATP, 0.42 mM phosphoenolpyruvate, 0.001 mM calcimycin (A23187, a Ca^{2+} ionophore), 0.2 mM NADH, 7.5 U/mL pyruvate kinase, and 18 U/mL lactate dehydrogenase (pH 7.5). Total hydrolytic activity was measured as the decrease of optical density at the NADH absorbance wavelength (340 nm) and expressed in micromoles of inorganic phosphate per milligrams of protein per minute (abbreviated as A.U.). The total hydrolytic activity of the HSR vesicles ranged from 6.05 to 6.8 A.U., and Ca^{2+}-dependent ATPase activity was identified as the portion of total hydrolytic activity inhibited by 5 μM thapsigargin (7). The toxin was added to the preparation 5 min before starting measurements of enzyme activity. The assay was performed in the presence of Ca^{2+} and EGTA mixtures, producing the estimated free Ca^{2+} concentration (2 μM) found to induce maximum SERCA activation.

Isolation of single skeletal muscle fibers

Single skeletal muscle fibers were isolated manually from the m. semitendinosus of frogs (*Rana esculenta*) as described previously (23). Briefly, the frogs were killed by rapid decapitation, followed by pithing. The fibers were mechanically separated in Ringer's solution (in mM, 115 NaCl, 2.5 KCI, 1.8 $CaCl_2$, and 5 HEPES) and then transferred to the recording chamber. The fibers were permeabilized by applying the following solution containing 0.004% saponin for 3 min (in mM, 100 K-glutamate, 10 HEPES, 1 EGTA, 5 $MgCl_2$, 5 Na_2-ATP, 10 sodium phosphocreatine, 10 glucose, 0.13 $CaCl_2$ and 8% dextran, 0.05 Fluo-3). After permeabilization the saponin was removed and 100 μM Fluo-4 was applied. The pH of the solutions was set to 7.0.

Single skeletal muscle fibers from the extensor digitorum communis muscles of rats were isolated enzymatically as described previously (23). Briefly, rats of either sex were anesthetized and killed by cervical dislocation. The muscles were removed and treated with collagenase 1.5 mg/mL (Sigma, Type I) for 1–1.5 hr at 37°C. The fibers were allowed to rest for at least 20 min after dissociation. Each selected fiber was transferred to a recording chamber filled with relaxing solution (in mM, 150 K-glutamate, 10 HEPES, 1 EGTA, 2 $MgCl_2$). The surface membrane was permeabilized using a relaxing solution (in mM, 125 potassium glutamate, 10 HEPES, 1 EGTA, 5 $MgCl_2$, 5 Na2-ATP, 10 sodium phosphocreatine, 10 glucose, 0.13 $CaCl_2$ and 8% dextran, 0.05 mM Fluo-3) containing 0.002% saponin. This solution was then changed to a K_2SO_4-based internal solution (in mM, 95 K_2SO_4, 10 Hepes, 1 EGTA, 6 $MgCl_2$, 5 Na_2-ATP, 10 sodium phosphocreatine, 10 glucose, 0.26 $CaCl_2$, 0.1 Fluo-4, and 8% dextran). The pH of the solutions was set to 7.2. The MCa and its mutants were added from 1 mM stock solution. The animals were killed in accordance with the guidelines of the European Community (86/609/EEC) following a protocol approved by the institutional animal care committee.

Measurement of elementary calcium release events

Fibers were imaged with an LSM 510 META laser scanning confocal microscope (Zeiss, Oberkochen, Germany) as reported previously (7). Line-scan images of fluorescence ($F(x,t)$) were taken at 1.54 ms line^{-1} and 512 pixels line^{-1} (pixel size 0.142 μm) parallel to the fiber axis. Fluo-4 was excited at 488 nm and emitted light was collected through a band-pass filter and digitized at 12 bit. Elementary calcium release events (ECRE) were captured using an automatic computer detection method (e.g., Cheng et al. (24)) as described in our previous report (7). The eventless portion of the image was used to calculate baseline fluorescence ($F_0(x)$). The program also determined the amplitude and as $\Delta F/F_0$, the spatial halfwidth measured at the time of the peak (full width at half-maximum (FWHM)) and duration for sparks, and the average amplitude, duration, and FWHM for embers. FWHM was calculated by fitting a Gaussian function to the spatial distribution obtained by averaging three lines at the peak for sparks, or by all lines except the first and last 10 ms of the event for embers.

Chemicals

Protease inhibitors were obtained from Boehringer (Mannheim, Germany), Fluo-3 and Fluo-4 were purchased from Molecular Probes Inc. (Eugene, OR, USA), and all other chemicals, unless otherwise specified, were obtained from Sigma (St. Louis, MO, USA).

RESULTS

Effect of the wild-type MCa on isolated RyR1

The effect of the MCa-RyR interaction on the channel function was tested using RyR1 incorporated into the planar lipid bilayer (Fig. 1). Applying 50 nM MCa on the cytoplasmic (*cis*) side of the channel induced LLSS, which corresponded to ~40% of the full conductance (Fig. 1 *B*). In the case of wild-type MCa, the subconductance state displayed an average LLSS time that was several thousand times longer than that of the mean open time of the unmodified channel (Fig. 1, *A* and *B*). Between LLSS, in the presence of the peptide, the channel showed normal gating with increased activity. This manifested as an ~10-fold increase in the open probability during the inter-LLSS periods in the presence of 50 nM MCa *cis* ($P_{o,control} = 0.02 \pm 0.007$; $P_{o,MCa} = 0.21 \pm 0.016$). The channel retained its ohmic behavior during the inter-LLSS periods, as demonstrated by the linear current-voltage relationship presented in Fig. 1 *C*. This was not the case for the LLSS, as will be addressed below (see Fig. 3 *D*).

It is interesting that the MCa-modified channel retained its ryanodine sensitivity since MCa also induced a subconductance state of the ryanodine-modified RyR1 (Fig. 1 *D*). It should be stressed that in the parallel presence of ryanodine (1 μM) and MCa (200 nM), the effect of ryanodine was the determinant because the channel spent most of its time in the ''half-conductance state'' characteristic for ryanodine, which then alternated with the LLSS induced by the peptide. Note also that the conductance of the MCa-induced LLSS of the ryanodine-modified channel and that of the native channel were not equal. Rather, the wild-type peptide reduced the conductance to ~36% of the full conductance (see also Fig. 3 *C*) and again to ~36% of the already reduced (''half'') conductance, for the native and ryanodine-modified channels, respectively. The duration of the LLSS events was found to be independent of the peptide concentration in the 1–500 nM concentration range; only the time required to get the channel into the LLSS was concentration dependent (data not shown).

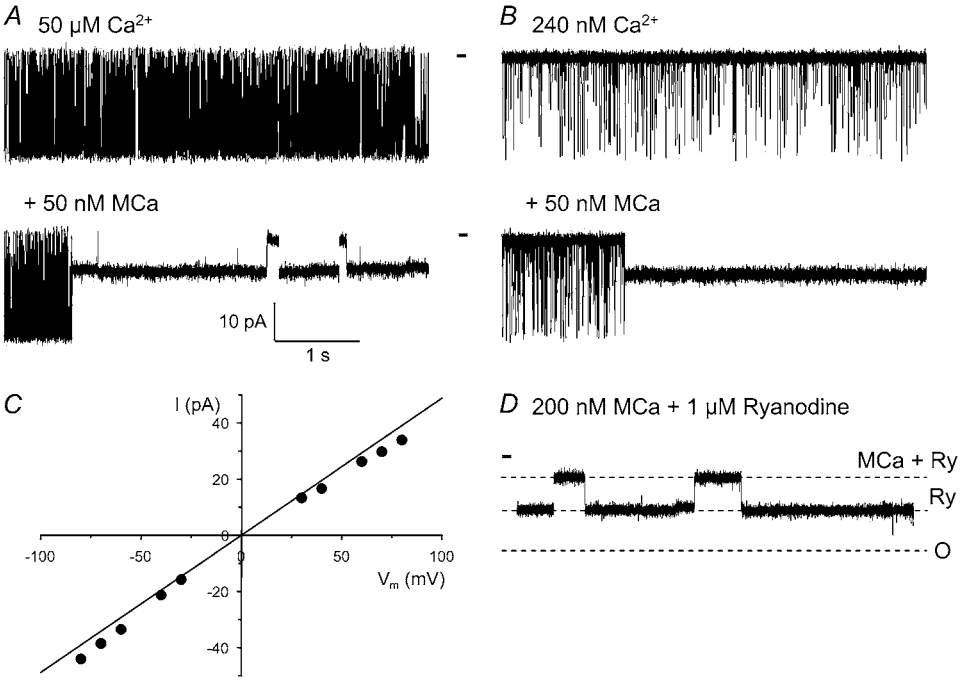

FIGURE 1 Effect of MCa and ryanodine on the calcium channel. The solubilized ryanodine receptor of the rat was incorporated into a lipid bilayer and the channel current was recorded under voltage clamp conditions using +55 mV as the holding potential at two different *cis* [Ca^{2+}] (50 μM, *left*; 240 nM, *right*). The charge carrier was 250 mM KCl; channel openings are represented by downward deflections. The closed state of the channel is marked between the current traces using the symbol —. (*A* and *B*) Single-channel recordings obtained under control conditions and in the presence of 200 nM MCa demonstrating the LLSS, lasting for several seconds, for the latter. (*C*) Current-voltage relationship for the full conductance state calculated from records in the presence of MCa. (*D*) Recording in the presence of 200 nM MCa and 1 μM ryanodine (50 μM [Ca^{2+}] *cis*). The ryanodine-induced specific half conductance state is labeled as Ry, whereas the MCa-induced state in the presence of ryanodine is labeled as MCa + Ry. For reference the full open state is also marked with O.

Effects of mutated analogs of MCa on the isolated RyR1

If, by analogy with other peptide toxin-ion channel associations (25–27), the high-affinity MCa-RyR1 interaction is mediated by electrostatic forces, mutations in the interaction domain of MCa should alter its electrostatic potential and/or the pattern of the subconductance states. Fig. 2 demonstrates that synthetic MCa derivatives activate the isolated RyR and induce subconductance states, in a similar fashion (but to different extents) to the wild-type MCa. Mutations within the cluster of basic amino acids of residues 20–24 elicited dramatic effects. Replacing ^{24}Arg with Ala ([Ala^{24}]MCa mutant) in MCa's sequence essentially abolished the MCa-induced subconductance states (Fig. 2 *G*). Mutants [Ala^{20}]MCa, [Ala^{22}]MCa, and [Ala^{23}]MCa exhibited consequently shorter and shorter transitions to the subconductance state, paralleling the putative 3D distance (28,29) of their mutation with respect to residue 24 (Fig. 2, *D–F*). In contrast, replacing Lys8 or Lys19 with Ala yielded almost the same LLSS as did the wild-type MCa (Fig. 2, *B* and *C*). Not only the temporal characteristics but also the relative amplitude of the subconductance state varied with the mutation, with the wild-type peptide producing the smallest conductance.

Effects of wild-type MCa and its mutated analogs on Ca^{2+}-ATPase activity

We also tested whether the peptides would alter the function of the SR calcium pump. Neither the wild-type toxin nor any of its mutants exhibited any effect on the hydrolytic activity

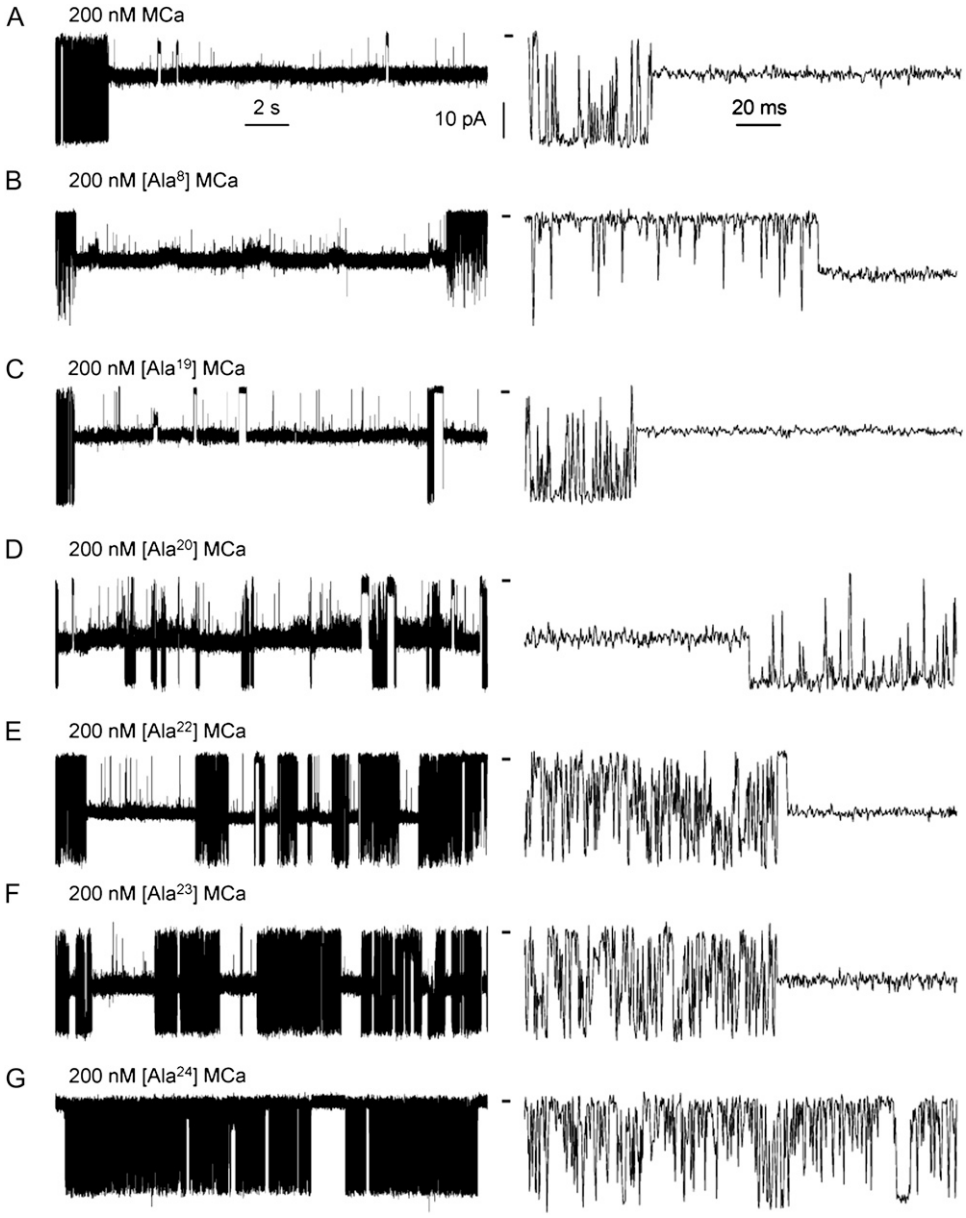

FIGURE 2 Effect of MCa and its mutants on the RyR1 of the rat. (*A–G*) Representative current traces in the presence of MCa (*A*) and its mutants (*B–G*; as marked). Experimental conditions are identical to those for Fig. 1 *A*. The traces in the left and right columns show identical single-channel recordings obtained using different time scales to better visualize the effects of different mutants. Between the two columns the closed state is marked as —. Note that when the place of the mutation is closer to the critical residue ^{24}Arg, the length and the frequency of LLSS decrease while the single-channel conductance corresponding to the full openings of the channel does not change.

of the Ca^{2+}-ATPase (Supplementary Material, Fig. S1 and Fig. S2).

MCa mutants alter the channel gating in two different ways

The effects of the peptide, in the presence of 240 nM ionized calcium, on the LLSS ratio—the relative time the channel spends in LLSS (see Materials and Methods)—and the length of these events are demonstrated in Fig. 3, *A* and *B*. As the site of the mutation became closer and closer to the critical residue 24, the LLSS ratio became smaller and smaller (Fig. 3 *A*). Furthermore, the place of the mutation affected the average LLSS event length more substantially than the LLSS ratio (Fig. 3 *B*). Note also that the LLSS ratio as well as the frequency of the events increased along with the peptide concentration. The average length of the LLSS events, on the other hand, seemed to be independent of the peptide concentration (Fig. 3 *B*).

In addition to affecting the time that channels spend in the LLSS, the mutation altered the relative conductance (the conductance of LLSS as normalized to the full conductance of the channel) as well (Fig. 3 *C*). Although the wild-type peptide reduced the conductance to 35.2% ± 3.7% during the LLSS, other mutants had increasingly smaller effects, again paralleling the spatial distance of their mutation in the putative 3D structure of the peptide.

Polarity dependence of the effects of MCa

The data presented in Fig. 3, *A–C* were obtained with a holding potential of +55 mV. It is important to stress here that the parameters of the LLSS events induced by MCa and its mutants depended on the polarity, and in some cases on the actual value, of the membrane potential, that is, on the direction of the current. When the charge carrier (K^+ or Ca^{2+}) moves from the *trans* to the *cis* side, the current direction is identical to that observed when calcium is released from the SR (''physiological direction''). Using membrane potentials (negative holding potentials) to drive the ions in the physiological direction, the LLSS ratios for each and every mutant were found to be lower as compared to the opposite polarity (''reverse direction''; Table 1). The effect of the peptides, in this respect, appeared to be independent of the actual value of the holding potential in the voltage range of 20–120 mV; only the polarity (current direction) had an appreciable effect. It is also interesting that the effect of MCa on the LLSS ratio was identical at 50 μM and 240 nM free

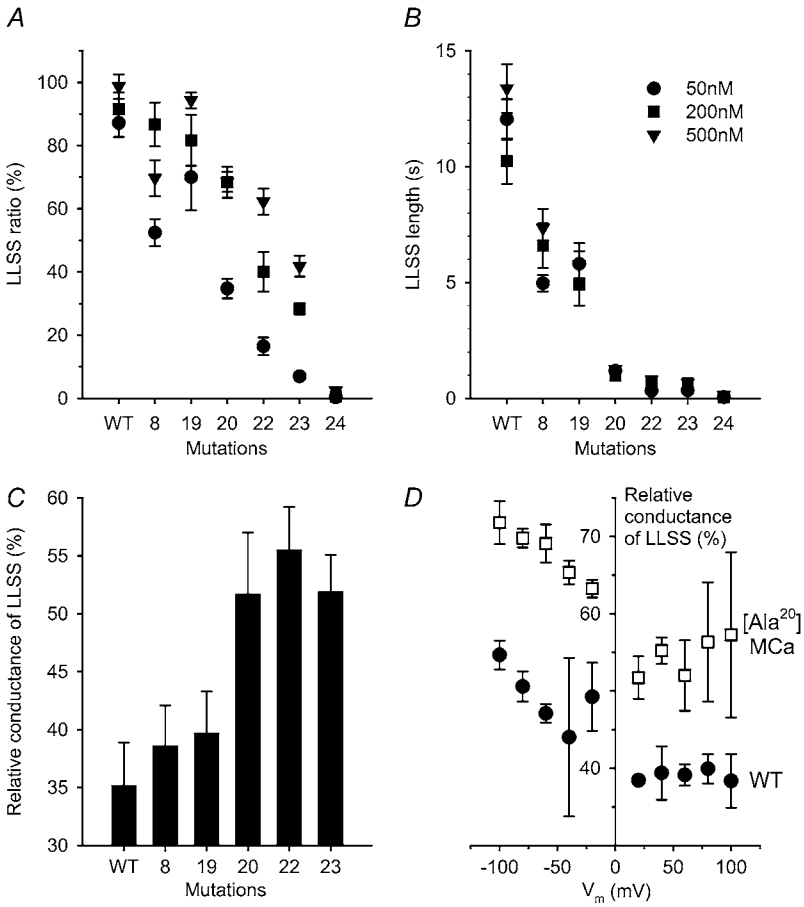

FIGURE 3 Parameters of the LLSS differ for different mutants. (*A* and *B*) Single-channel records were taken at 50 nM (●),200 nM (■), and 500 nM (▼) peptide concentrations, and the LLSS ratio (*A*) and average length of the LLSS events (*B*) were determined. The LLSS ratio was calculated as the ratio of the time spent in the subconductance state over the total time and expressed as percentage. Note that when the site of the mutation is placed more and more distant from the critical residue ^{24}Arg, the channel spends less and less time in the LLSS state. Note also that although the concentration of the peptide did influence the LLSS ratio, it had little effect, if any, on its average length. (*C*) Relative conductance of LLSS for the different mutants was calculated by normalizing the conductance of LLSS to that of the full conductance state. Measurements for panels *A–C* were taken at the holding potential of +55 mV; each symbol represents the mean of at least 20 events taken from at least eight bilayers. (*D*) Voltage dependence of the relative conductance of LLSS for the wild-type MCa (●; 25 nM) and the [Ala^{22}]MCa mutant (□; 250 nM). Values are expressed as a percentage of the full conductance state in panels *C* and *D*.

TABLE 1 Polarity and concentration dependence of LLSS ratio with different MCa mutants

MCa analog	[peptide] (nM)	Reverse direction	Physiological direction*
wild-type	50	88.1 ± 10.5	9.8 ± 1.1
	200	91.5 ± 11.2	43.8 ± 5.2†
[Ala^{8}]MCa	50	52.5 ± 6.1	3.5 ± 0.74
	200	86.7 ± 9.1†	5.4 ± 0.60†
[Ala^{20}]MCa	50	34.8 ± 6.4	3.1 ± 0.72
	200	68.4 ± 8.2†	3.9 ± 0.63
[Ala^{24}]MCa	50	0.34 ± 0.18	not detected
	200	0.62 ± 0.21	not detected

*Physiological direction was defined as the direction in which calcium moves during its release from the SR. The LLSS ratio was determined as described in Materials and Methods and expressed as percentage.
†Indicates that the difference is significant ($p < 0.01$) between the LLSS ratios determined at 50 nM and 200 nM peptide concentration.

calcium concentration in the case of the wild-type MCa (Fig. 1, *A* and *B*) and the [Ala^{8}]MCa mutant, whereas it was slightly lower at low calcium for the other mutants. The length of LLSS was also calcium independent in both current directions (data not shown).

On the other hand, the relative conductance of the MCa-modified channel displayed a clear voltage dependence for the wild-type MCa and all mutated analogs, similar to that presented for MCa and [Ala^{20}]MCa in Fig. 3 *D*. The voltage dependence was present at negative potentials, with a greater conductance at negative holding potentials as compared to the same but positive holding potentials. The relative conductance increased essentially linearly as the holding potential was moved further and further away from 0 mV, indicating again that the effect of the peptides was current-dependent. The wild-type peptide behaved similarly to its mutated analogs at both holding potentials.

To test whether the parameters of the LLSS induced by MCa depend on the presence of an externally applied voltage or on the actual flow of the charge carrier, we tested the effect of the wild-type peptide using a symmetrical (250 mM / 250 mM) charge carrier situation with an externally applied 40 mV membrane potential and an asymmetrical (50 mM / 250 mM) K^+ concentration (corresponding to the same driving force according to the Nernst equation). The former represents the current driven by the electrical field (i.e., potential difference), whereas the latter represents the charge transfer driven by the concentration gradient (measured at zero membrane potential) determined as the short circuit current. These experiments, using the wild-type MCa, revealed that the membrane potential and the concentration gradient—generating the same current—resulted in similar parameters for the LLSS events (data not shown).

These results highlight the existence of a localized binding site of MCa on RyRs and suggest that the MCa-RyR interaction can be modified with the place of the mutation. To further investigate the effect of the different mutations of MCa at the level of EC coupling, ECREs were studied on adult skeletal muscle fibers.

Effects of MCa analogs on event properties of permeabilized mammalian fibers

We have previously shown that MCa can initiate or modify the properties of spontaneous calcium release events in adult mammalian striated muscle fibers (14). We thus tested whether the different mutants of MCa would alter calcium release in a manner similar to their effect on isolated channels. To this end, cells from rat skeletal muscle were permeabilized, placed in a sulfate-based internal solution containing Fluo-4, and imaged with a confocal scanner. Fibers showed spontaneous calcium release events (Fig. 4 *A*) in accordance with previous observations (5,6,14). Shortly after the addition of 50 nM MCa (2–10 min), the frequency at which ECRE occurred increased considerably (Fig. 4 *B*). In addition to sparks, long openings with or without sparks were also observed (Fig. 4 *B*, inset). To test the specificity of the mutants of MCa, we added the [Ala^{8}]MCa analog of MCa, which was found to have similar effects on the occurrence

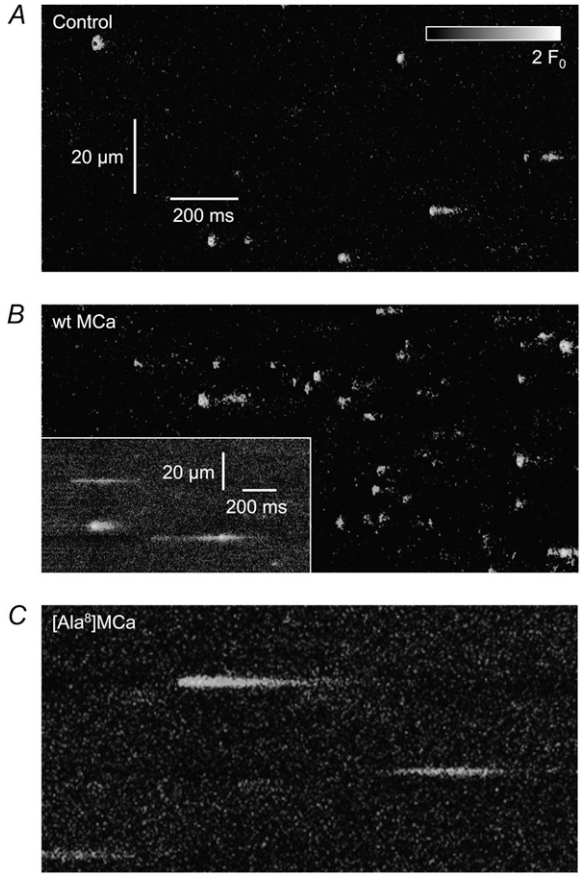

FIGURE 4 Effect of wild-type and mutant MCa on calcium release events in rat skeletal muscle fibers. Line-scan images in control (*A*) and in the presence of wild-type MCa (*B*) and [Ala^{8}]MCa mutant (*C*) in saponin-skinned rat skeletal muscle fibers. Scanning was made parallel with the fiber axis. Images were corrected for background fluorescence (F/F_0) and pseudo-colored. Note the larger number of long-lasting embers as compared to control in the presence of both types of the peptide. The inset shows that wild-type MCa causes similar long events as the [Ala^{8}]MCa mutant.

(Fig. 4 *C*) and duration (187 ± 4 vs. 185 ± 3 ms, $n = 767$ and 1109, for MCa and the mutant, respectively) of embers as the wild-type peptide.

It should be stressed that the above averages are lower estimates of the actual average durations in the presence of the peptides since they inevitably contain durations from events that originate from nonmodified channels. This can be appreciated clearly from the histograms presented in Fig. 5 *A*, where the distribution of event duration is displayed for control fibers and for cells treated with 50 nM MCa. Note that under control conditions the event duration never exceeded 250 ms, whereas in the presence of the peptide events with durations over 250 ms are clearly present. Nevertheless, the majority (95%) of events in the presence of MCa had durations shorter than 250 ms. These latter events most likely originate from nonmodified channels since at this low concentration of the peptide the channel spends less than 10% of its time in the MCa-modified state (see Table 1). To overcome this problem, we also measured the duration of events in the presence of 1 μM MCa, where the majority of events should represent the peptide-modified channels. Fig. 5 *B* demonstrates that the distribution of event duration in the presence of such a high peptide concentration is clearly altered as compared to that in the control. The events with short duration are now suppressed and long events dominate, that is, 15.4% of all events have durations exceeding 1 s (Fig. 5 *B*, *inset*). Although one can still not exclude the possibility that events from MCa-modified channels with durations shorter than 250 ms are still present, their contribution should be greatly reduced. Therefore, to estimate the average duration of these events, we used the above criteria and obtained 1072 ± 49 ms ($n = 459$).

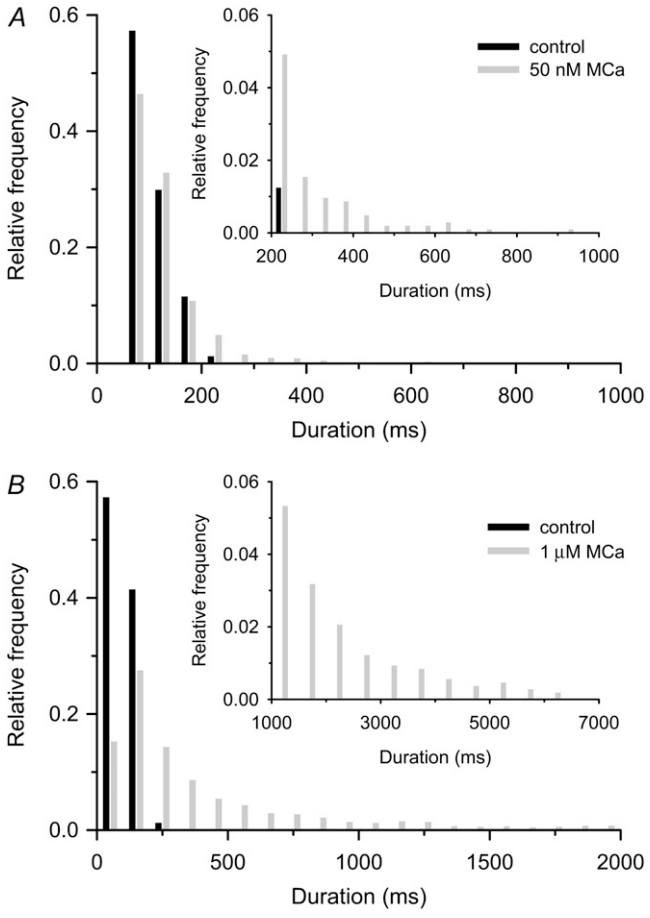

FIGURE 5 Relative distribution of ember durations. (*A*) Event durations were measured under control conditions (*black bars*) and in the presence of 50 nM MCa (*gray bars*). Note the presence of events longer than 250 ms in the presence of the peptide, which were not observed under control conditions. Inset shows the distribution at an expanded *y*-scale for better visualization of the longer events. (*B*) Event durations in the absence and presence of 1 μM of MCa. Note the clear alteration in the shape of the distribution in the presence of the peptide. Inset again shows the distribution at an extended *y*-scale.

To capture events with durations of several seconds in the presence of MCa or the Ala^{19} mutant (see Fig. 6 *A* for an example of the latter), longer imaging times were used. However, to avoid photo-damaging the cells unnecessarily, this was not done routinely. It is also intriguing that, unlike in frogs (see below), where a spark preceded the long ember, the events in rats always started as a sudden step to an increased fluorescence level, which was then maintained during the entire event.

Occasionally (22 events out of 344), however, stepwise changes in fluorescence were detectable, as presented in Fig. 6 *B*. The amplitudes of these steps were slightly greater than the original 158% ± 18% for the second step as normalized to the first, indicating either the opening of an additional but independently gated channel or the transition to the fully conducting state. Although we have no direct evidence to support the latter, it is intriguing to note that the step to the full conductance state from the LLSS in isolated channels was also ~150% of the LLSS state (see, e.g., Fig. 2 or 3 *C*). In addition to simple stepwise changes in fluorescence, events with complex kinetics were also captured (Fig. 6 *B*, *b*). These showed long openings, lasting for several hundreds of milliseconds that alternated with a burst-like pattern clearly resembling that seen for isolated channels (Fig. 2).

Effects of MCa analogs on amphibian fibers

While mammalian fibers readily produce calcium release events of long duration and small amplitude under control conditions, amphibian fibers are normally devoid of such events. To further explore the effects of the mutations of MCa and derive quantitative measures for their duration, we used permeabilized frog skeletal muscle fibers, in which a long event with small amplitude would clearly mark a peptide-modified channel. Fig. 7 thus presents line-scan images recorded under control conditions (Fig. 7 *A*) and in the presence of wild-type MCa, $[Ala^{8}]$MCa, $[Ala^{19}]$MCa, and $[Ala^{22}]$MCa (Fig. 7, *B–E*, respectively). The wild-type peptide and the mutants decreased event frequency but produced long-lasting calcium release events that were

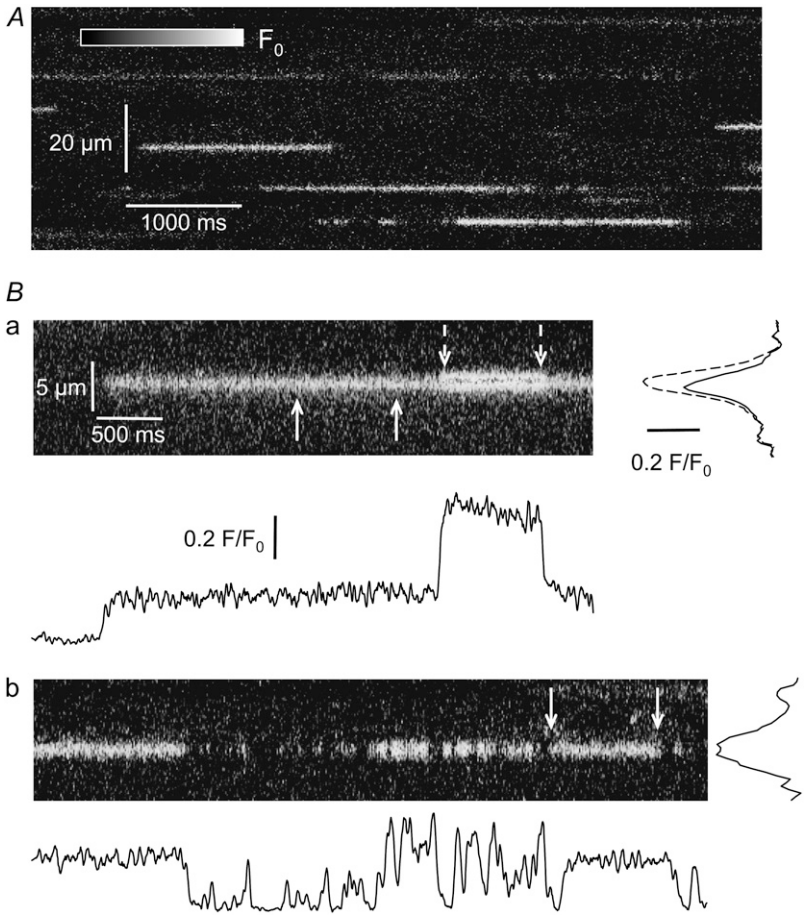

FIGURE 6 Long-lasting calcium events caused by the [Ala^{19}]MCa mutant in rat skeletal muscle fibers. (*A*) Pseudo-colored line-scan image taken in the presence of [Ala^{19}]MCa. The same scanning direction and image correction were applied as in Fig. 4, but the length of acquisition was eight times longer. Note the very long event durations and the presence of endless events on either side of the image. (*B*, *a*) A representative ember with a secondary opening taken from a long scan. (*B*, *b*) A representative event demonstrating the successive reopenings of the channel. The traces below the images show the average of five neighboring lines at the middle of the event, and the traces next to the images represent the spatial spread of the event calculated by averaging the lines between the times marked by white arrows. The solid and dashed traces in panel *B*, *a* correspond to the time windows marked by solid and dashed arrows with calculated FWHMs of 1.54 and 1.44 μm during and before the secondary opening, respectively.

never observed under control conditions in frogs but resembled those reported for IpTxA (30). In line with data from single channels, the [Ala^{22}]MCa mutant caused shorter calcium release events than those produced by the other two mutants (see also Fig. 8 *A*).

Note also that these long events seem to always start with a ''classical'' spark. From the several thousand long events measured in the presence of MCa or its mutants, only a handful (such as the one presented in the inset of Fig. 7 *B* for the wild-type MCa) had no leading spark.

The mutation of MCa alters the morphology of ECRE

We found similar effects of the different mutants of MCa on the length of embers in permeabilized frog skeletal muscle fibers as was shown above on LLSS length. As shown in Fig. 8 *A*, the mutants [Ala^{8}]MCa and [Ala^{19}]MCa were almost as effective as the wild-type MCa at both 50 and 100 nM. In contrast, the [Ala^{22}]MCa mutant induced ~60% and 50% shorter events than did the native peptide at the two concentrations, respectively. We also tested [Ala^{24}]MCa, but in the presence of this analog we did not observe embers as in the peptide-free control solution (data not shown).

As mentioned above, the peptide-modified events, in most cases, displayed a starting spark followed by a prolonged ember. Fig. 8 *B* plots the amplitude and FWHM, as a measure of the spatial spread, of these components for the wild-type peptide. The events that were assumed to be the closest to the confocal plane, as judged by their large amplitude, were selected from those included in panel *A*. As shown in Fig. 8 *B*, the starting sparks had five to six times greater amplitudes and slightly larger FWHMs than the trailing embers.

DISCUSSION

In this work we evaluated how the replacement of different amino acids in the sequence of the wild-type MCa affects its ability to modify the gating of the skeletal-type RyR. We show that mutations of MCa within the cluster of positively charged residues surrounding ^{24}Arg decrease the appearance of LLSS on isolated channels reconstituted into planar lipid bilayers and long-lasting embers in saponin-treated adult striated muscle fibers. The extent of this effect depended on the direction of the current in lipid bilayer experiments, indicating a current- and voltage-dependent interaction of the peptide with the channel.

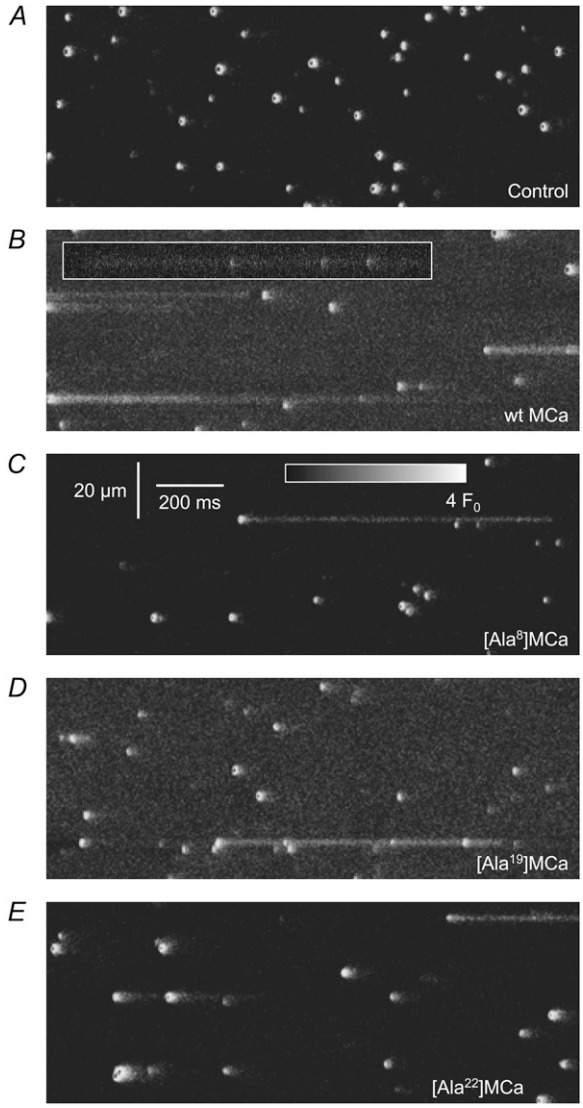

FIGURE 7 Effect of wild-type and mutant MCa on calcium release events in frog skeletal muscle fibers. Pseudo-colored line-scan images under control conditions (*A*) and in the presence of wild-type MCa (*B*) and [Ala^{8}]MCa (*C*), [Ala^{19}]MCa (*D*), and [Ala^{22}]MCa (*E*) mutants in frog skeletal muscle fibers. The same scanning direction and image correction were applied as in Fig. 4. Note the decreased number of long-lasting embers in the presence of [Ala^{22}]MCa as compared to those measured in the presence of wild-type MCa and the other mutants. The inset in panel *B* displays a rare event in which the long opening was not preceded by a spark.

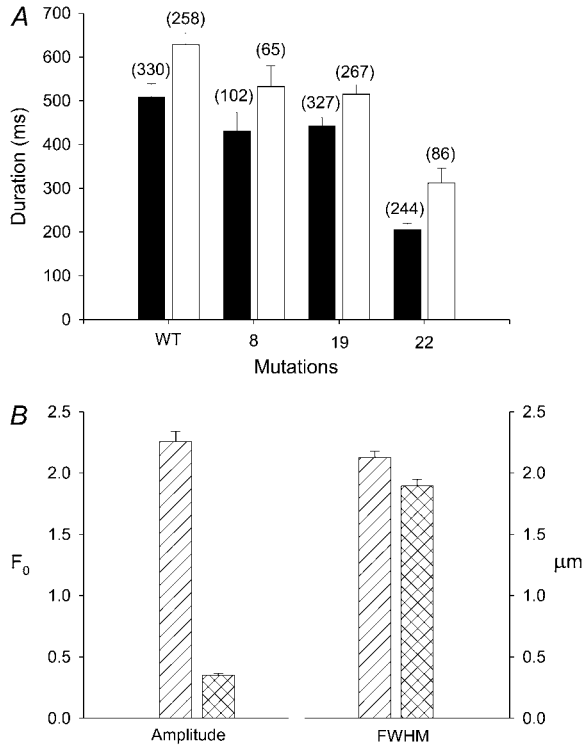

FIGURE 8 Effect of MCa and its mutants on the parameters of calcium release events. (*A*) The average length of the events measured in the presence of wild-type MCa and its different mutants calculated from images similar to those presented in Fig. 7. Empty bars represent averages measured in the presence of 50 nM, and filled bars give values in the presence of 100 nM of the peptides. The numbers above the bars give the number of events included in the average. Only those events whose lengths could reliably be estimated were considered. Note the fewer number of events for the [Ala^{22}]MCa mutant. (*B*) The parameters of the leading spark (*hatched bars*) and the trailing ember (*cross-hatched bars*) for selected large events ($n = 66$) measured in the presence of the wild-type peptide (50 nM). In the case of the trailing ember, the average amplitude is given.

Effect of mutations in MCa on the lengths of LLSS and ECRE

In previous studies we have demonstrated that MCa increases the frequency of ECRE together with a decrease in the amplitude of the individual events in saponin-treated adult mammalian striated muscle fibers (14). In addition, it induces long-lasting embers with durations that usually exceed 200 ms and occasionally last longer than 1.5 s. On purified RyR1 reconstituted into planar lipid bilayers, the peptide induced both an increase in the open probability of the channel and the appearance of long-lasting open events characterized by a reduced conductance (12,13). As a consequence of these effects, MCa caused a dramatic increase in the [^{3}H]ryanodine binding to RyR1, as well as in Ca^{2+} release from SR vesicles. All of these effects were completely abolished by the point mutation of the Arg residue in position 24 of MCa (13,14), supporting the hypothesis that the basic amino acid-rich region is important for the functional effect of MCa on RyR1.

Here we show that the effects of MCa described for LLSS and ECRE depend on the position of mutation of the peptide and correlate with the putative spatial distance of the mutation from the charged surface of MCa as derived from the suggested 3D structure of the peptide (29). Indeed, the effects of [Ala^{8}]MCa and [Ala^{19}]MCa mutants on ECRE were almost identical to those of the wild-type peptide. In the presence of [Ala^{22}]MCa, the length of embers decreased, whereas the [Ala^{24}]MCa analog did not show any effect on ECRE. These results are in direct agreement with the observations originating from lipid bilayer experiments, with these analogs illustrating that the capability for inducing the

LLSS of RyR1 depends on the location of the mutation in the structure.

Changing amino acids at different positions, by substituting a charged amino acid with a neutral one, thus reveals that the dramatic effect of the mutations within the putative 3D cluster of basic amino acids (Fig. 9, *A* and *B*) cannot be solely attributed to the change of the net electrical charge of the peptide since mutations that were distant to the cluster but produced the same change in net electrical charge had relatively minor effects. Since structural changes within MCa due to its triple disulphide bonds are unlikely to accompany the mutations, this cluster is the most likely candidate for the interacting site with the RyR.

The properties of the MCa binding site on RyR

Recent evidence has positioned the MCa binding site to residues 3351–3507 on RyR1 (31). The results presented here suggest that the peptide binding site is distant from the high-affinity calcium binding (regulatory) site because the effects of the peptides were essentially calcium-independent. In addition, it also appears to be distinct from the ryanodine binding site (see below). Finally, it should be noted that the calcium release channel, when gating to the full conductance state, was still ohmic after binding MCa or its mutants, indicating, for this effect, an allosteric modification of the RyR conformation by the peptides.

The fact that the LLSS length was found to be independent of the concentration of MCa, or the concentration of its analogs, suggests that one MCa binds to an RyR channel. On the other hand, the fact that the inter LLSS open probability is higher (by ~10-fold) than under control conditions indicates that an alternative binding site, presumably four on the tetrameric channel, is a precondition for the occupation of the fifth (''in pore'' or central) binding site, for this special type of gating.

Given the above constraints and the reasonable assumption that MCa and its mutants bind to RyR1 via a common structural motif, the corresponding mutations should evoke parallel changes in the affinity if the continuity of the basic surface is essential. Since this was confirmed in all measurements, we can conclude that the orientation of the peptide is likely to be the most important factor in determining its binding to the site that is responsible for the initiation of LLSS, probably because the electric field-induced orientation of the peptide plays an important role in its binding to (or interaction with) the channel. This suggests that this MCa binding site is near the opening of the channel pore, where the electric gradient is extremely large, and thus the electric momentum dominates the orientation of the MCa molecule. In the above framework, due to the necessity of a suitable orientation of the charged surface, the interaction of MCa with the RyR should be influenced by the polarity of the membrane potential. In line with the above reasoning, we

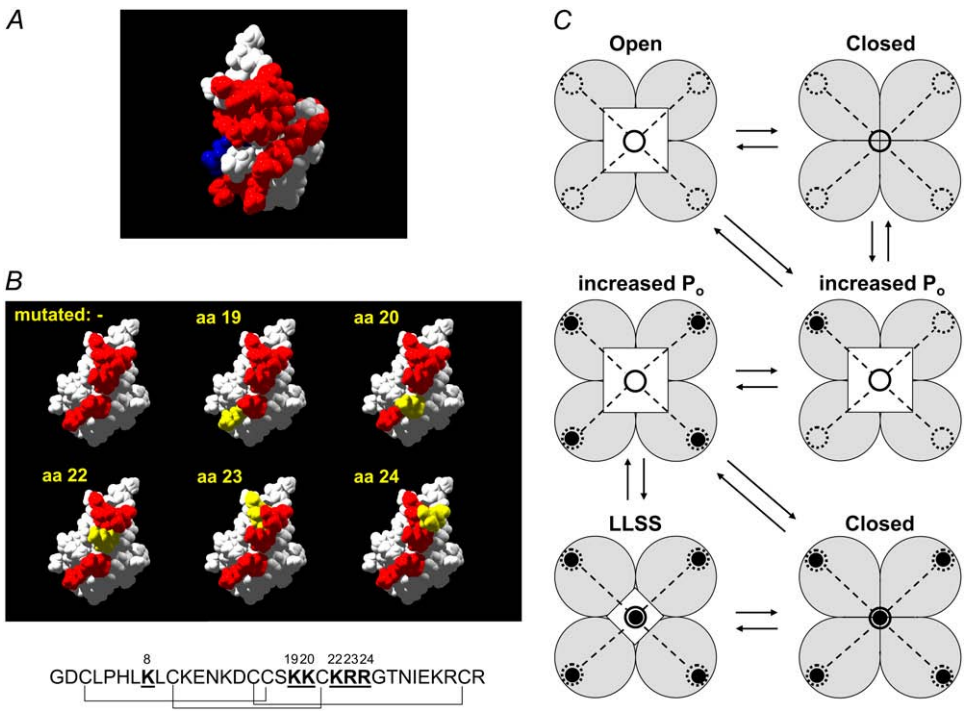

FIGURE 9 3D structure and proposed binding sites of MCa. (*A*) Putative 3D structure of MCa with the basic amino acids (aa) colored red, the acidic aa colored blue, and all others colored white. The presented 3D structure is based on NMR measurements reflecting the structure of the molecule dissolved in an aqueous phase (29). (*B*) Predicted 3D structure of the wild-type and mutated peptides together with the aa sequence. In the first image, the red color shows positively charged aa whose mutations were tested in this study; all other aa are in white. The yellow color in all subsequent images represents the actually mutated aa; these were only recolored without recalculation of the structure. (*C*) Proposed model for the MCa binding sites on the functional channel unit. Each RyR1 monomer has one (identical) binding site (*dotted circles*) and the tetramer has an extra—collective—site (solid circle) positioned in the central part of the channel. Open circles represent unoccupied MCa binding sites, and filled circles represent occupied MCa binding sites. The area of the white central square, the pore, is proportional to the conductance of the channel under the given condition.

found that the dissociation constants of the peptides were polarity-dependent.

We thus propose a model (Fig. 9 *C*) in which four binding sites are located far from the pore on the RyR tetramer (one on each monomer), altering the open probability of the channel in a voltage-independent manner (characterized by normal type of gating). The fifth binding site would, in this framework, be responsible for the potential-dependent (current-direction dependent) LLSS (see Table 1. and Fig. 3.), which is expected to be in the very vicinity of the vestibule of the pore, and must be in direct relation with the other four, as confirmed by the finding that LLSS were always preceded by increased open probability. Once the putative binding site within the pore is occupied, the channel can gate between the LLSS and the closed state, as seen clearly in Fig. 1 *A* for the wild-type MCa and in Fig. 2 *C* for the [Ala^{19}]MCa mutant. Occasionally the channel swaps back to normal gating with higher activity (Fig. 2). This model is also supported by the finding that only the time required to get the channel into the subconductance state varies with the concentration of the peptides. In the case of the wild-type toxin, this was found to be in the 20 min to 20 s range for toxin concentrations in the 1–500 nM range. This type of dose dependence is not unique, being similar to the effect of ryanodine on RyR1 and also to the effect of cyclopiazonic acid on the Ca^{2+} ATPase.

We recently suggested that in intact cells MCa binds preferably to the RyR after its activation via the DHPR (15). It should be noted that this conclusion was derived by comparing the prolonged calcium release after repolarization with that of maximal calcium release during the depolarizing pulse. This prolonged calcium release should correspond to the LLSS seen in lipid bilayer experiments. This suggests that the binding site for the peptide that is responsible for the induction of LLSS is inaccessible or less accessible when the channel is closed. Clearly, a binding site within or in close association to the channel pore would fulfill this criterion. If the binding site is indeed found within the pore, the movement of positively charged ions through the channel (the calcium release process) should hinder the binding of the positively charged peptide. A similar phenomenon is expected to take place in bilayer experiments if the holding potential is set to drive the charge carrying ions in the physiological direction. This is indeed what was observed, strengthening the idea that the binding site is somehow associated with the pore itself.

Combined effect of ryanodine and MCa

Normally, low concentrations of ryanodine induce a characteristic half-conductance state of RyR from which the channel only occasionally closes, and only for a short time (for a few milliseconds), and it never switches back to the full open state unless the ryanodine is removed from the bathing solution (for review see Meissner and el-Hashem (32)). In the case of the simultaneous presence of ryanodine and MCa, the half-conductance state characteristic of the alkaloid dominates channel behavior. Nevertheless, long closing periods due to the presence of MCa become apparent, during which the channel enters a further reduced conductance state, clearly indicating that the binding of the peptide and the alkaloid are independent of one another. The apparently free gating of the channel between these two states ensures that although the binding of MCa or ryanodine might influence the binding of the other, the state into which MCa transforms the channel is independent of that induced by ryanodine.

The binding site for MCa and its effect on ECRE

MCa and its structural analog IpTxA have been shown to induce extremely long calcium release events in amphibian skeletal muscle fibers (14,28,33). These events are most likely a direct consequence of the calcium release channel entering into the LLSS after the binding of the peptide. Several pieces of evidence support this conclusion. First, the length of these long events correlates well with the length of LLSS. We obtained 1.1 s for the average duration of the long embers (Fig. 5 *B*), which should be compared with the average length of LLSS given in Fig. 3 *B* (12 s; wild-type MCa). Note, however, that the values in Fig. 3 were obtained with a positive holding potential (reverse direction of the current; Table 1), whereas in the fiber current flow is in the physiological direction. Second, mutations in MCa caused parallel changes in the ability of the peptide to induce LLSS on isolated channels and to modify the kinetics of ECRE. Third, stepwise changes in event amplitude were observed in peptide-treated cells. Whereas such events were not seen under control conditions, they have been reported for K-201, an immunophylin capable of inducing subconductance states in RyR1 (34). These stepwise changes could be explained by a sudden change in release and/or removal of calcium. Since a very rapid change is unlikely occur in the calcium binding sites (in their concentration or affinity for calcium) within the myoplasm, a possible candidate could be an MCa-induced alteration in the properties of the calcium pump—a reduction in the amount of calcium transported into the SR. However, neither MCa nor its mutated analogs seem to exert any effect on the ATP-ase activity of the calcium pump (Fig. S1 and Fig. S2). This leaves us with the possibility that calcium release is altered suddenly, due either to the opening of an additional channel (or channels) or an increase in the conductance of an already open channel. Whereas we cannot exclude the possibility that the opening of neighboring channel(s) caused the sudden increase, the correlation between the magnitude of the change and the relative conductance of the LLSS as well as the minimal change in FWHM argue in favor of the latter possibility. Finally, neither the wild-type MCa nor its mutated analogs had any effects on the SR calcium pump (data not shown). This, on the one hand, clearly confirms that these long events are a result of the calcium released through a single peptide-modified channel

whereas calcium sparks are generated by the opening of a group of calcium release channels. On the other hand, it gives further insight into the interaction of MCa and the calcium release channel. As discussed above, the peptide seems to prefer the open conformation when it interacts with RyR. If MCa binds only to the open channel, the prediction would be that long events should tail calcium sparks. This is clearly the case for amphibians, in which long events are generally made up of a leading spark and a trailing ember. It should be noted, however, that a few events (2% of those in which long embers were observed) are devoid of the leading ember. This indicates that there is a possibility, albeit a much lower one, for the peptide to bind to the closed channel. We, of course, cannot exclude the possibility that the binding actually occurred right after the opening of the channel and this event then prevented neighboring channels from opening and the spark from being formed. Whereas this scenario is an acceptable, although unlikely, possibility in amphibians, it clearly cannot account for the observation that in mammals all long events are without leading sparks. Taken together, our data are in line with the hypothesis that MCa and its mutants bind preferably but not solely to the open channel.

SUPPLEMENTARY MATERIAL

To view all of the supplemental files associated with this article, visit www.biophysj.org.

The authors are grateful for the technical assistance of Ms R. Őri and Ms É. Sági.

The work was supported by grants from the Hungarian Scientific Research Fund OTKA (T049151, NK61412, K61442).

REFERENCES

1. Tsugorka, A., E. Rios, and L. A. Blatter. 1995. Imaging elementary events of calcium release in skeletal muscle cells. *Science*. 269:1723–1726.
2. Klein, M. G., H. Cheng, L. F. Santana, Y. H. Jang, W. J. Lederer, and M. F. Schneider. 1996. Two mechanisms of quantized calcium release in skeletal muscle. *Nature*. 379:455–458.
3. Gonzalez, A., W. G. Kirsch, N. Shirokova, G. Pizarro, M. D. Stern, and E. Rios. 2000. The park and its ember: separately gated local components of Ca^{2+} release in skeletal muscle. *J. Gen. Physiol.* 115:139–157.
4. Shirokova, N., J. Garcia, and E. Rios. 1998. Local calcium release in mammalian skeletal muscle. *J. Physiol.* 512:377–384.
5. Kirsch, W. G., D. Uttenweiler, and R. H. A. Fink. 2001. Spark- and ember-like elementary Ca^{2+} release events in skinned fibers of adult mammalian skeletal muscle. *J. Physiol.* 537:379–389.
6. Zhou, J., G. Brum, A. Gonzalez, B. S. Launikonis, M. D. Stern, and E. Rios. 2003. Ca^{2+} sparks and embers of mammalian muscles. Properties of the sources. *J. Gen. Physiol.* 122:95–114.
7. Szentesi, P., H. Szappanos, C. Szegedi, M. Gönczi, I. Jona, J. Cseri, L. Kovacs, and L. Csernoch. 2004. Altered elementary calcium release events and enhanced calcium release by thymol in rat skeletal muscle. *Biophys. J.* 86:1436–1453.
8. Marx, S. O., K. Ondrias, and A. R. Marks. 1998. Coupled gating between individual muscle Ca^{2+} release channels (ryanodine receptors). *Science*. 281:818–821.
9. El-Hayek, R., A. J. Lokuta, C. Arevalo, and H. H. Valdivia. 1995. Peptide probe of ryanodine receptor function. Imperatoxin A, a peptide from the venom of the scorpion *Pandinus imperator*, selectively activates skeletal-type ryanodine receptor isoforms. *J. Biol. Chem.* 270: 28696–28704.
10. Fajloun, Z., R. Kharrat, L. Chen, C. Lecomte, E. Di Luccio, D. Bichet, M. El Ayeb, H. Rochat, P. D. Allen, I. N. Pessah, M. DeWaard, and J. M. Sabatier. 2000. Chemical synthesis and characterization of maurocalcine, a scorpion toxin that activates Ca^{2+} release channel/ryanodine receptors. *FEBS Lett.* 469:179–185.
11. Shahbazzadeh, D., N. Srairi-Abid, W. Feng, N. Ram, L. Borchani, M. Ronjat, A. Akbari, I. N. Pessah, M. De Waard, and M. El Ayeb. 2007. Hemicalcin, a new toxin from the Iranian scorpion *Hemiscorpius lepturus* which is active on ryanodine-sensitive Ca^{2+} channels. *Biochem. J.* 404:89–96.
12. Chen, L., E. Estève, J. M. Sabatier, M. Ronjat, M. DeWaard, P. D. Allen, and I. N. Pessah. 2003. Maurocalcine and peptide A stabilize distinct subconductance states of ryanodine receptor type 1, revealing a proportional gating mechanism. *J. Biol. Chem.* 278:16095–16106.
13. Estève, E., S. Smida-Rezgui, S. Sarkozi, C. Szegedi, I. Regaya, L. Chen, X. Altafaj, H. Rochat, P. D. Allen, I. N. Pessah, I. Marty, J. M. Sabatier, I. Jona, M. DeWaard, and M. Ronjat. 2003. Critical amino acid residues determine the binding affinity and the Ca^{2+} release efficacy of maurocalcine in skeletal muscle cells. *J. Biol. Chem.* 278:37823–37831.
14. Szappanos, H., S. Smida-Rezgui, J. Cseri, C. Simut, J. M. Sabatier, M. De Waard, L. Kovacs, L. Csernoch, and M. Ronjat. 2005. Differential effects of maurocalcine on Ca^{2+} release events and depolarization-induced Ca^{2+} release in rat skeletal muscle. *J. Physiol.* 565:843–853.
15. Pouvreau, S., L. Csernoch, B. Allard, J. M. Sabatier, M. De Waard, M. Ronjat, and V. Jacquemond. 2006. Transient loss of voltage control of Ca^{2+} release in the presence of maurocalcine in skeletal muscle. *Biophys. J.* 91:2206–2215.
16. Szentesi, P., J. Almássy, M. Fehér, B. Dienes, C. A. Simut, I. Jona, M. Ronjat, and L. Csernoch. 2006. Mutation in the scorpiotoxin maurocalcine alter its ability to modify the calcium release events in frog skeletal muscle. *J. Muscle Res. Cell Motil.* 27:516–517.
17. Merrifield, B. 1986. Solid phase synthesis. *Science*. 232:341–347.
18. Lai, F. A., and G. Meissner. 1990. Structure of the calcium release channel of skeletal muscle sarcoplasmic reticulum and its regulation by calcium. *Adv. Exp. Med. Biol.* 269:73–77.
19. Sarkozi, S., C. Szegedi, B. Lukacs, M. Ronjat, and I. Jona. 2005. Effect of gadolinium on the ryanodine receptor/sarcoplasmic reticulum calcium release channel of skeletal muscle. *FEBS J.* 272:464–471.
20. Lai, F. A., H. P. Erickson, E. Rousseau, Q. Y. Liu, and G. Meissner. 1988. Purification and reconstitution of the calcium release channel from skeletal muscle. *Nature*. 331:315–319.
21. Herrmann-Frank, A., M. Richter, S. Sarkozi, U. Mohr, and F. Lehmann-Horn. 1996. 4-Chloro-m-cresol, a potent and specific activator of the skeletal muscle ryanodine receptor. *Biochim. Biophys. Acta*. 1289:31–40.
22. Fabiato, A. 1988. Computer programs for calculating total from specified free or free from specified total ionic concentrations in aqueous solutions containing multiple metals and ligands. *Methods Enzymol.* 157:378–417.
23. Szentesi, P., V. Jacquemond, L. Kovacs, and L. Csernoch. 1997. Intramembrane charge movement and sarcoplasmic calcium release in enzymatically isolated mammalian skeletal muscle fibers. *J. Physiol.* 505:371–384.
24. Cheng, H., L. S. Song, N. Shirokova, A. Gonzalez, E. G. Lakatta, E. Rios, and M. D. Stern. 1999. Amplitude distribution of calcium sparks in confocal images: theory and studies with an automatic detection method. *Biophys. J.* 76:606–617.
25. Hidalgo, P., and R. MacKinnon. 1995. Revealing the architecture of a K^+ channel pore through mutant cycles with a peptide inhibitor. *Science*. 268:307–310.
26. Dudley, S. C., H. Todt, G. Lipkind, and H. A. Fozzard. 1995. A muconotoxin-insensitive Na^+ channel mutant: possible localization of a binding site at the outer vestibule. *Biophys. J.* 69:1657–1665.

27. Gurrola, G. B., C. Arevalo, R. Sreekumar, A. J. Lokuta, J. W. Walker, and H. H. Valdivia. 1999. Activation of ryanodine receptors by imperatoxin A and a peptide segment of the II–III loop of the dihydropyridine receptor. *J. Biol. Chem.* 274:7879–7886.

28. Mosbah, A., R. Kharrat, Z. Fajloun, J. G. Renisio, E. Blanc, J. M. Sabatier, M. El Ayeb, and H. Darbon. 2000. A new fold in the scorpion toxin family, associated with an activity on a ryanodine-sensitive calcium channel. *Proteins.* 40:436–442.

29. Lee, C. W., E. H. Lee, K. Takeuchi, H. Takahashi, I. Shimada, K. Sato, S. Y. Shin, D. H. Kim, and J. I. Kim. 2004. Molecular basis of the high-affinity activation of type 1 ryanodine receptors by imperatoxin A. *Biochem. J.* 377:385–394.

30. Shtifman, A., C. W. Ward, J. Wang, H. H. Valdivia, and M. F. Schneider. 2000. Effect of imperatoxin A on local sarcoplasmic reticulum Ca^{2+} release in frog skeletal muscle. *Biophys. J.* 79:814–827.

31. Altafaj, X., W. Cheng, E. Estève, J. Urbani, D. Grunwald, J. M. Sabatier, R. Coronado, M. DeWaard, and M. Ronjat. 2005. Maurocalcine and domain A of the II–III loop of the dihydropyridine receptor Cav 1.1 subunit share common binding sites on the skeletal ryanodine receptor. *J. Biol. Chem.* 280:4013–4016.

32. Meissner, G., and A. el-Hashem. 1992. Ryanodine as a functional probe of the skeletal muscle sarcoplasmic reticulum Ca^{2+} release channel. *Mol. Cell. Biochem.* 114:119–123.

33. Gonzalez, A., W. G. Kirsch, N. Shirokova, G. Pizarro, G. Brum, I. N. Pessah, M. D. Stern, H. Cheng, and E. Rios. 2000. Involvement of multiple intracellular release channels in calcium sparks of skeletal muscle. *Proc. Natl. Acad. Sci. USA.* 97:4380–4385.

34. Almassy, J., M. Sztretye, B. Lukacs, B. Dienes, L. Szabo, P. Szentesi, G. Vassort, L. Csernoch, and I. Jona. 2008. Effects of K-201 on the calcium pump and calcium release channel of rat skeletal muscle. *Pflugers Arch.* 10.1007/s00424–008–0504–7.